https://doi.org/10.5194/egusphere-2026-109
Preprint. Discussion started: 19 February 2026

Detecting long-term canopy change and vegetation shifts in northern peatlands using LAI and climate data

Iuliia Burdun [1, 2], Jiabin Pu [3], Ranga B. Myneni [3], Miina Rautiainen [1]

[1] School of Engineering, Aalto University, Espoo, Finland
[2] Department of Earth and Environmental Sciences, KU Leuven, Heverlee, Belgium
[3] Department of Earth and Environment, Boston University, Boston, MA, United States of America

Correspondence to: Miina Rautiainen (miina.a.rautiainen@aalto.fi)

Abstract. Peatlands store vast amounts of carbon, yet their canopies are changing under northern warming. We assessed recent vegetation trajectories by analysing greening and browning across northern peatlands using a gap-filled, sensor-independent climate data record of leaf area index (LAI) for 2001–2023. To our knowledge, this provides the first multi-decadal, peatland-specific assessment of canopy trends based strictly on mapped peatlands. Although greening was widespread at the pixel level (77% of peatlands; greening-to-browning ratio 3.5:1), the area-weighted LAI trend at the map scale was not significant. LAI anomalies were weakly positively correlated with temperature and weakly negatively correlated with precipitation. Higher tree cover was associated with less greening, with a smaller effect observed in areas with deciduous needleleaf forests and under higher precipitation. Decadal variability left a regional, non-linear imprint: most pixels showed no breakpoints, but where present they often were temporally aligned with phase shifts in the Pacific Decadal Oscillation (PDO). Cup-shaped trends were concentrated in West Siberia, whereas hat-shaped trends were widespread across Europe, northeastern Asia, and Canada. Protected peatlands did not show different LAI trends when differences in climate and canopy were taken into account. Overall, recent peatland canopy change was not a uniform increase in greenness but reflected moisture-sensitive, composition-dependent responses modulated by decadal climate variability. Together, these results provide a circumpolar, peatland-specific baseline that clarifies where and why LAI is changing and enables evaluation of how moisture conditions, decadal variability, canopy composition, and protection status relate to recent canopy trajectories in northern peatlands.

1 Introduction

Peatlands have helped cool our climate by an estimated 0.6 °C over the Holocene by sequestering carbon (C) from the atmosphere and storing it as peat (United Nations Environment Programme, 2022). These ecosystems are built and sustained by plants that engineer waterlogged, nutrient-poor, anoxic conditions. When those conditions shift, such as under a warming, drying climate, plant communities reorganise (Liu et al., 2023), altering the processes that regulate peatland C dynamics (Bansal et al., 2023; Virkkala et al., 2025; Yuan et al., 2024). Peatlands may consequently shift from C sinks to sources (Bansal et al., 2023), especially in northern regions (north of 45° N), where rapid warming (Qiu et al., 2022) has contributed to widespread drying of peatlands (Swindles et al., 2019).

https://doi.org/10.5194/egusphere-2026-109
Preprint. Discussion started: 19 February 2026

Across the northern regions, warming has already led to increases in vegetation height, biomass, cover, and abundance (Myers-Smith et al., 2020), and expanded colonisable areas following the drainage of permafrost lake basins (Chen et al., 2023). Within this broader context, northern peatlands stand out because their environment is strongly self-engineered by vegetation, particularly *Sphagnum*, the dominant peat former, which is highly sensitive to temperature (Campbell et al., 2021; Oke and Hager, 2017), partly because warming alters its metabolic composition (Sytiuk et al., 2023). As suitable habitats decline, *Sphagnum* is projected to migrate northwards (Ma et al., 2022), increasing the risk of invasion by vascular plants (Ma et al., 2022; Oke et al., 2020) that can reduce peatland productivity and C sequestration (Bragazza et al., 2012; Keane et al., 2025). Consistent with these projections, case studies have shown local-scale shifts in peatland vegetation driven by warming (Elmendorf et al., 2012; Kolari et al., 2021; Sturm et al., 2001), related wildfires (Väliranta et al., 2017) and changes in snow cover (Backéus et al., 2023), with species changes detected even within strictly protected areas (Ren et al., 2021).

Because these changes occur over decades and across continental scales, only satellite remote sensing enables consistent monitoring of vegetation properties, including canopy greenness, structure, and productivity (Myers-Smith et al., 2020). Building on these observations, long-term satellite archives have revealed areas of increasing ("greening") and decreasing ("browning") vegetation activity (Myneni et al., 1997). Since the early 1990s, browning has expanded markedly—by more than 60%—across northern latitudes, leading to widespread greening-to-browning reversals and a slowdown in global greening, despite overall greening dominance since the early 1980s (Pan et al., 2018; Winkler et al., 2021). Although greening and browning dynamics have been widely investigated, large-scale studies have generally not addressed peatlands as a distinct ecosystem (Higgins et al., 2023) or have excluded them from the analysis (Winkler et al., 2019; Xu et al., 2013). Consequently, global and semi-global mapping of greening and browning trends has mostly been focused on other ecosystem types (Barichivich et al., 2013; Cai et al., 2025; Forzieri et al., 2017; Lian et al., 2020; Piao et al., 2019; Zhu et al., 2016), leaving how vegetation trends evolve over decades across the full extent of northern peatlands unclear and limiting the ability to anticipate responses to environmental changes, assess resilience, and guide management.

Here, we address this gap by analysing greening and browning across northern peatlands over the past two decades, using a gap-filled, sensor-independent climate data record (CDR) of leaf area index (LAI). This provides, to our knowledge, the first multi-decadal, peatland-specific assessment of canopy trends based strictly on mapped peatlands, rather than generic boreal or Arctic ecosystems. We apply the Partitioned Autoregressive Time Series (PARTS) approach, which accounts for both spatial and temporal autocorrelation, to robustly link observed LAI trends to potential drivers. Our study addresses two research questions:

(1) What are the spatial and temporal patterns of greening and browning in northern peatlands over the past two decades? and
(2) Do climatic, ecological, and protection-related factors explain these patterns?

We hypothesise that northern peatlands exhibit spatially coherent greening or browning trends in LAI and that these trends can be explained by (i) climate-related changes, including warming, precipitation and recent lake drainage in the northern permafrost zone; (ii) differences in protection status; and (iii) variation in tree cover type and density.

https://doi.org/10.5194/egusphere-2026-109
Preprint. Discussion started: 19 February 2026

2 Data

2.1 Polygons of northern peatlands

The potential distribution of peatlands has been the focus of several recent global mapping efforts (Fluet-Chouinard et al., 2023; Hu et al., 2017; Hugelius et al., 2020; Xu et al., 2018). One of the most widely used datasets, PEATMAP (Xu et al., 2018), has been shown to underestimate the northern peatland extent by roughly 1 million km² (Hugelius et al., 2020). The recently released Global Peatland Map 2.0 (Anon, 2024) offers improved coverage and consistency at a spatial resolution of 1 km; however, this coarse grid limits its direct integration with satellite datasets of finer spatial resolution.

To overcome these limitations, we integrated the following four complementary datasets to map peatlands north of 45 °N: (i) PEATMAP, which includes polygons of peatlands (Xu et al., 2018)); (ii) Open Street Map (OSM) for which we derived polygons tagged as "Wetland" (OpenStreetMap, 2025) downloaded on 02 May 2024; (iii) ESA WorldCover 2021 – global land cover product at 10 m resolution, based on Sentinel-1 and 2 data, for which we derived pixels classified as "Herbaceous wetland" (class 90); and (iv) Global Peatland Map 2.0 – 1 km resolution that indicates locations of peatlands.

Because the OSM and ESA WorldCover datasets map wetlands rather than specifically peatlands (peatlands are a type of wetland), our first step was to retain only those wetland locations that intersect with the Global Peatland Map 2.0. We applied the same intersection to PEATMAP, although it directly represents peatlands, to ensure a consistent and systematic workflow across all datasets. From these intersected layers, we retained only areas represented in at least two of the three datasets (OSM, PEATMAP, and ESA WorldCover), and finally aggregated the resulting areas (Fig. 1). This approach was designed to minimise potential biases arising from the limitations of individual datasets, while acknowledging that OSM coverage is uneven and often sparse in areas with few active contributors.

2.2 Sensor-independent leaf area index climate data record for northern peatlands

We used sensor-independent LAI CDR at 500 m spatial and 8-day temporal resolution for 2001-2023 (Pu et al., 2024). This dataset was selected for its low mean absolute error, comparable to the high-quality LAI retrievals of original MODIS Terra/Aqua/VIIRS LAI products (Pu et al., 2024). This dataset also includes data on the fraction of photosynthetically active radiation (FPAR); however, because spatial patterns of greening and browning in FPAR closely matched those observed for LAI (Fig. A1), we focus our results on LAI only. The LAI data were obtained in the MODIS sinusoidal projection, and all other datasets in this study were reprojected accordingly to ensure spatial consistency.

For each LAI pixel, we calculated the proportion of area covered by mapped peatlands, as derived in Section 2.1, and retained only those with peatland coverage of 90% or greater. To minimise confounding effects from rapid vegetation changes following wildfires, we excluded all pixels classified as burned between 2001 and 2023 in the combined Terra and Aqua MCD64A1 dataset version 061. MCD64A1 data were accessed and processed in the Google Earth Engine cloud-based platform. The final number of pixels for our analysis was 1,244,063 (Fig. 1).

https://doi.org/10.5194/egusphere-2026-109
Preprint. Discussion started: 19 February 2026

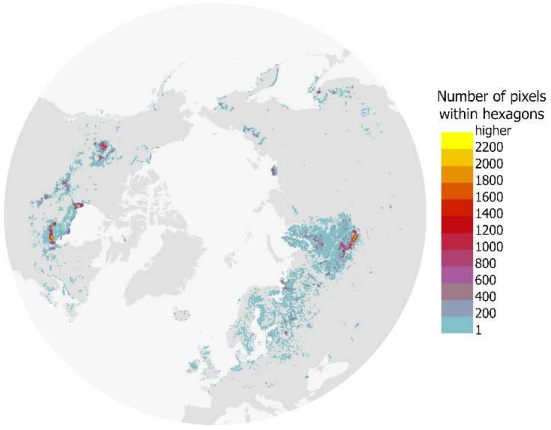

Figure 1: Study area and number of 500 m resolution pixels from the sensor-independent leaf area index raster within each 500 km² hexagon used for visualisation.

100

2.3 Climatic, ecological, and protection-related data

2.3.1 Climatic information

To characterise a broad-scale climatic regime affecting peatland vegetation patterns, we used the present-day Köppen-Geiger climate dataset (Beck et al., 2018). In our study area, the climate classes varied between 5 (BWk: Arid, desert, cold) and 29 (ET: Polar, Tundra) with most of the pixels having climate 27 (Dfc: Cold, no dry season, cold summer – 985,441 pixels) and 26 (Dfb: Cold, no dry season, warm summer – 151,789 pixels). For analysis, the original classes were aggregated into four main groups: Dry (classes 5-7), Temperate (classes 8-16), Continental (classes 17-28), and Polar (class 29).

To represent multi-year to decadal climate variability potentially influencing vegetation, we used monthly Pacific Decadal Oscillation (PDO) index data for 2001-2023 (Pacific Decadal Oscillation (PDO) | National Centers for Environmental Information (NCEI), 2025). PDO has a relatively strong impact on changes in temperature and precipitation in the region north of 40°N and can weaken or enhance greening trends (Guo et al., 2023). During the preliminary analysis, we examined monthly data for the Arctic Oscillation (AO), North Atlantic Oscillation (NAO), and Oceanic Niño Index (ANOM34), in addition to the PDO index. We estimated pixel-based Pearson correlations between detrended anomalies of LAI and those indices with a time lag from 0 to 6 months. Since the PDO without time lag had the highest absolute values of the Pearson correlation coefficient (ranging from -0.33 to 0.37), we used it in further analysis.

Finally, to capture spatial variability and long-term trends in key meteorological parameters, we used ERA5 reanalysis daily mean temperature of air at 2m above the surface of land and total precipitation for 2001-2023 (Hersbach et al., 2020).

https://doi.org/10.5194/egusphere-2026-109
Preprint. Discussion started: 19 February 2026

2.3.2 Tree canopy cover and type

We used the global tree cover dataset for the year 2000, defined as canopy closure for all vegetation taller than 5 m and expressed as a percentage per grid cell (Hansen et al., 2013), to calculate the mean tree cover for each of the studied pixels. To identify the potential tree-cover type present in the studied pixels, we used the MCD12Q1.061 annual land cover product at 500 m spatial resolution for 2001 as a baseline at the start of the analysis period. Land Cover Type 1, based on the International Geosphere–Biosphere Programme classification, was filtered to retain only the tree-cover classes. After that, we calculated planar Euclidean distances to identify the nearest pixel belonging to one of the retained classes and assigned its tree-cover type, ensuring that every studied pixel had an attributed potential nearest tree-cover class :

1. evergreen needleleaf forests included 488,104 pixels;
2. evergreen broadleaf forests included 1,703 pixels;
3. deciduous needleleaf forests included 173,534 pixels;
4. deciduous broadleaf forests included 90,972 pixels; and
5. mixed forests included 489,750 pixels.

Classes 2 and 4 were merged because evergreen broadleaf forests (class 2) contained very few studied pixels. Assigning potential tree-cover type using the nearest-class distance matrix introduces some uncertainty, but it provides spatially complete coverage while retaining the broader landscape context of surrounding vegetation, offering a consistent solution for large-scale analyses. Nevertheless, the distances between pixel centroids and the nearest tree cover varied widely, which introduces uncertainty in these assignments: class 1- mean 19 km (max 346 km), class 2 - 2 km (16 km), class 3 - 27 km (252 km), class 4 - 15 km (337 km), and class 5 - 4 km (254 km). Therefore, these forest-type effects should be further interpreted with appropriate caution. While many northern peatlands are naturally treeless, we assigned a potential tree-cover type to all pixels to enable its use in the analysis as an interaction term with tree-cover percentage, without implying the actual presence of trees in treeless areas (Figure A2).

2.3.3 Elevation and continent information

We derived the elevation for each centroid of the studied pixels using a dataset from SRTM data (Fick and Hijmans, 2017). The elevation of the studied pixels varied from -32 m to 1619 m. Additionally, we included continent information to account for continental differences in vegetation sensitivity to climatic parameters (Muccio et al., 2025). To assign each peatland pixel to a continent, we obtained country boundaries from the *rnaturalearth* database (Natural Earth vector and raster map data, 2025), and split the Russian Federation along the 60° E meridian, treating the territory east of this line as Asia and the territory to the west as Europe.

https://doi.org/10.5194/egusphere-2026-109
Preprint. Discussion started: 19 February 2026

2.3.4 Areas of Arctic lake drainage

We used the Arctic drained lake dataset (Chen et al., 2023) to identify the studied pixels with documented lake drainage events after 2001, allowing us to test whether such hydrological disturbances within peatland-dominated pixels were associated with distinct LAI trajectories.

2.3.5 Protection status of peatlands

Using the World Database on Protected Areas (downloaded April 2024), we classified each studied pixel into one of three protection categories:

1. Protected – pixels entirely within protected areas established before 2000 (136,999 pixels);
2. Non-protected – pixels outside any protection area for the full period covered by the dataset (1,038,094 pixels);
3. Mixed – pixels either (i) within protected areas designated 2000, or (ii) partially overlapping both protected and unprotected areas between 2000 and 2023 (68,970 pixels).

We included all types of protection recognised in the dataset, regardless of designation level (national, regional, international, or not available) and legal status ("Designated", "Proposed", "Established"). This approach ensured that all areas under effective protection at the start of our 2001–2023 satellite record were represented, thereby avoiding the omission of sites that deliver real-world conservation outcomes despite legal designation delays. Only the polygon dataset was used; the point dataset was excluded, as just nine studied pixels included protected point sites of unknown area.

3 Methods

Our study comprised three main methodological steps: 1) extracting detrended anomalies from LAI and climate data and analysing their associations (Section 3.1), 2) detecting breakpoints in LAI anomalies (Section 3.2), and 3) estimating net long-term greening and browning trends in northern peatlands, complemented by spatially explicit hypothesis testing of factors influencing LAI change (Section 3.3). In this way, we separated descriptive trend analysis (Section 3.2) from inferential testing of net long-term linear trends and their covariate associations (Section 3.3). Inference, therefore, was made for map-scale linear trend responses, while breakpoint outputs were used for descriptive mapping of non-linear behaviour.

3.1 Extraction of anomalies in LAI and climate data and analysis of their associations

First, we removed long-term trends and seasonal components from the time series of LAI, air temperature, and precipitation for each pixel using the seasonal–trend decomposition by Loess (STL) implemented in R's base stats::stl function. We applied a periodic seasonal window and set the trend window to one year, decomposing the pixel-level time series into seasonal, trend, and remainder (r_t) components. The remainder was treated as the anomaly.

We then estimated pixel-level partial correlation, which quantifies the linear association between two variables while controlling for a third. Specifically, we calculated: (i) the partial correlation between LAI and air temperature anomalies,

https://doi.org/10.5194/egusphere-2026-109
Preprint. Discussion started: 19 February 2026

controlling for precipitation anomalies, and (ii) the partial correlation between LAI and precipitation anomalies, controlling for air temperature anomalies.

Finally, to assess the relationship between LAI anomalies and PDO, we averaged the LAI anomalies to monthly values and computed the Pearson correlation coefficient with the monthly PDO index.

3.2 Detecting breakpoints in LAI anomalies

A single long-term trend can mask periods of contrasting ecosystem behaviour. Therefore, following Higgins et al. (2021), we considered three possible LAI trend shapes: (i) hat-shaped, where LAI trend increased initially then decreased, (ii) cup-shaped, where LAI decreased initially and then increased, and (iii) linear, where no change in trend sign was detected. We restricted our analysis to a single breakpoint to capture the main turning point over 2001–2023. While multiple breakpoints can occur globally, higher northern latitudes were showed a higher share of zero and one trend change than lower latitudes (de Jong et al., 2012). Thus, the single-breakpoint model summarises the main change in direction, rather than implying that additional breakpoints cannot occur.

For each STL-derived anomaly time series r_t, we first detected linear and non-linear (cup-shaped and hat-shaped) trends fitting Bayesian polynomial regression with LaplacesDemon v. 16.1.6 :

$$r_t = b_0 + b_1 x_t + b_2 x_t^2 + \varepsilon_t,\ \varepsilon_t \sim N(0, \sigma^2), \quad (1)$$

where x_t is a time index in fractional years, standardised to zero mean and unit variance, b_0 – intercept, b_1 – linear trend coefficient, b_2 – curvature coefficient, ε_t – Gaussian noise with variance σ^2.

We specified weakly informative priors $b_0, b_1, b_2 \sim N(0, 10^3)$ and placed a $N(0,10)$ prior on $\log \sigma$, and recover the noise scale via $\sigma = \exp(\log \sigma)$, ensuring $\sigma > 0$. The Adaptive Metropolis–within–Gibbs ("AMWG") sampler was run for 600,000 iterations (thinning = 150). We recorded posterior means, standard deviations, 95% credible intervals (CI), overall acceptance rate, and deviance information criterion.

Second, if the quadratic curvature coefficient b_2 was estimated to be significant (its 95% CI did not include zero), we fitted the Bent-Cable model to identify the type of trend (hat-shaped or cup-shaped) and temporal location of the breaking point:

$$r_t = b_0 + b_1 x_t + b_2 q(x_t; \tau, \gamma), \quad (2)$$

where q is the bent-cable basis:

$$q(x; \tau, \gamma) = \begin{cases} 0, & x \le \tau - \gamma, \\ \frac{(x-(\tau-\gamma))^2}{4\gamma}, & \tau - \gamma < x < \tau + \gamma, \\ x - \tau + \gamma, & x \ge \tau + \gamma, \end{cases} \quad (3)$$

where $\tau \sim \text{Uniform}(Q_{0.15}, Q_{0.85})$ is a central change-point location in scaled time x within the central 70% of x, and $\gamma \sim \text{Uniform}(0,2)$ is a half-width of the transitional zone in scaled time units. We ran 30,000 AMWG iterations (thinning =150), rescaled τ back to the calendar date, and summarised posterior means and 95% CI.

https://doi.org/10.5194/egusphere-2026-109
Preprint. Discussion started: 19 February 2026

3.3 Estimating long-term linear greening and browning trends and testing of factors influencing LAI change

Long-term greening and browning trends of LAI were estimated using the remotePARTS package in R to account jointly for temporal and spatial autocorrelation across 1,244,063 pixels (Ives et al., 2021), thereby reducing sensitivity to autocorrelation in satellite time series (Ploton et al., 2020).

First, each pixel's LAI, air temperature, and precipitation series was modelled as a linear trend with AR(1) errors, obtaining restricted maximum likelihood estimates of unscaled trend coefficients via the fitAR_map() function. Second, the AR(1) residuals were used to estimate the range parameter of an exponential spatial covariance model. Third, for computational efficiency, 1,500-pixel partitions were analysed in parallel with fitGLS_partition(), fitting generalised least squares (GLS) models with exponential spatial covariance and a nugget per block. Block-level test statistics were then combined into an overall map-scale inference, controlling for spatial non-independence.

Finally, we tested whether: (i) LAI trends differed from zero across all pixels (net greening or browning), (ii) tree cover and type modulated LAI trends, (iii) protected peatlands exhibited distinct LAI trends compared to unprotected peatlands; (iv) LAI trends varied across climate zones and continents, latitude, longitude, and local air temperature and precipitation. We selected the final partitioned spatial GLS model by testing each candidate against its main-effects baseline using the remotePARTS pooled likelihood-ratio F-test, retaining the most parsimonious specification that significantly improved the fit. We prioritised interpretable, biophysically consistent interactions and excluded additions that offered negligible rSSE gains. The final model is shown in Table A1.

3.4 Visualisation

To minimise overplotting, we overlaid a grid of 500 km² hexagons on the raster data and, within each hexagon, calculated the mean of numerical values and the majority class for categorical data. These aggregated data were used only for plotting; analysis was conducted using non-aggregated data. These aggregated summaries are what we display on the manuscript's maps, with the total number of raster pixels within each hexagon shown in Fig. 1.

4 Results

4.1 Associations of LAI with air temperature, precipitation, and the PDO index

To study the association between peatlands' LAI and its potential climate drivers, we estimated spatial partial correlations between LAI anomalies and air temperature, precipitation, and the PDO index. Anomalies in LAI showed a weak but predominantly positive partial correlation with air temperature anomalies (Fig. 2a) and a weak, predominantly negative partial correlation with precipitation anomalies (Fig. 2b). Notably, the regions with the strongest associations were similar in both cases, with prominent patterns in West Siberia and the Hudson Bay Lowlands. The correlation between LAI anomalies and

https://doi.org/10.5194/egusphere-2026-109
Preprint. Discussion started: 19 February 2026

235 the PDO index yielded a spatially patchy pattern, with a broad positive correlation in southern West Siberia and the European part of Russia, and negative correlations in northern Europe and scattered areas in the Canadian Interior Plains (Fig. 2c).

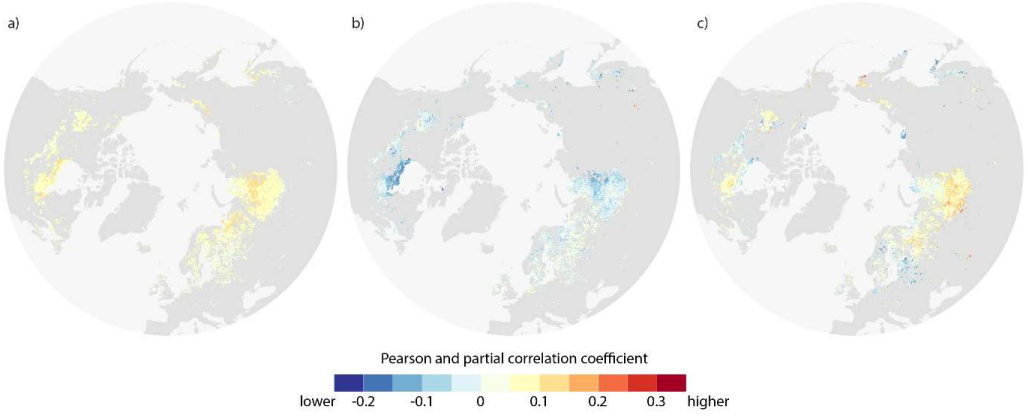

Figure 2: Spatial patterns of correlation between monthly anomalies of leaf area index (LAI) and potential climate drivers across northern peatlands during 2001–2023. (a) Partial correlation between LAI anomalies and air temperature anomalies, controlling 240 **for precipitation anomalies. (b) Partial correlation between LAI anomalies and precipitation anomalies, controlling for air temperature anomalies. (c) Pearson correlation between monthly LAI anomalies and the Pacific Decadal Oscillation (PDO) index. Colours indicate correlation coefficients, with the same scale applied to both Pearson and partial correlations.**

4.2 Shifts in LAI trends

The spatial distribution of LAI anomaly trend shapes revealed clear regional patterns (Fig. 3a). Linear trends dominated large 245 areas, cup-shaped trends were concentrated in West Siberia, and hat-shaped trends were widespread across Europe, Northeastern Asia and Canada. In West Siberia, a north–south gradient was evident: cup-shaped in the north, mainly linear in the middle, and hat-shaped primarily in the south.

Annual mean LAI anomalies also differed by trend shape (Fig. 3b). For the cup-shaped trends, anomalies declined during 2005–2010, and the density of posterior mean breaking point peaked earlier (2005–2010) than in the hat-shaped class. For the 250 hat-shaped trends, anomalies rose to a maximum around 2010–2015 and then decreased, with a later peak in breaking point density (2012–2016). In both non-linear classes, peaks in breaking point density occurred soon after a phase change in the PDO.

https://doi.org/10.5194/egusphere-2026-109
Preprint. Discussion started: 19 February 2026

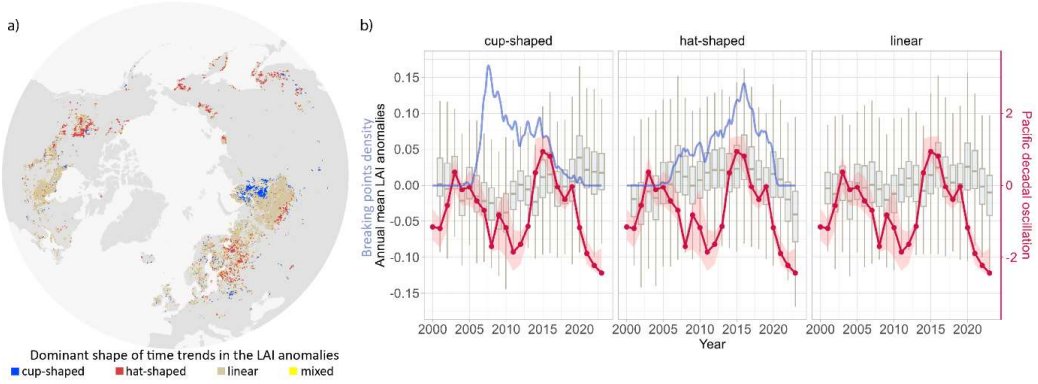

Figure 3: Spatial and temporal patterns of dominant LAI anomaly trends in northern peatlands. (a) Spatial distribution of the dominant trend shape in LAI anomalies, classified as cup-shaped, hat-shaped, linear, or mixed (where two or more shapes occurred with equal frequency within a hexagon). (b) Annual mean LAI anomalies (box plots) for pixels belonging to each trend type, overlaid with the density of posterior mean breakpoint years (blue line; higher values indicate more pixels with a breakpoint in that year) and the Pacific Decadal Oscillation (PDO) index (red line; shaded area shows 25–75% quantiles).

4.3 Decadal LAI trends

Out of the studied northern peatlands, covering approximately 261,819 km², more than 77% (203,269 km²) exhibited positive LAI trends, while the rest (approximately 58,550 km²) showed negative trends (Fig. 4a). The strongest positive decadal LAI trends clustered in southern West Siberia, Central Europe, and southern Fennoscandia. The largest pattern of negative LAI trends was located near Hudson Bay Lowlands in North America. Overall, the LAI trends in peatlands vary from -1.07 to 0.78 $m^2m^{-2}decade^{-1}$, with 95% of values ranging from -0.07 to 0.09 $m^2m^{-2}decade^{-1}$. Across the frequency of mean decadal LAI trends, the relative contribution of the three trend shapes was broadly similar (Fig. 4b).

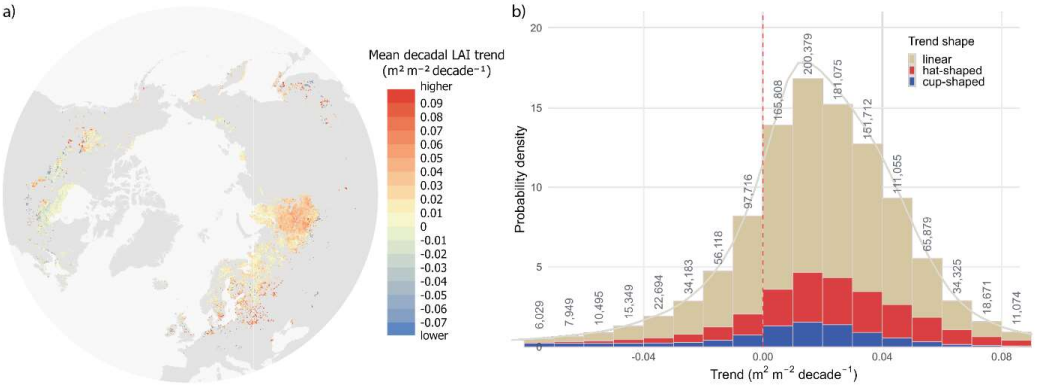

Figure 4: Spatial distribution and frequency of mean decadal LAI trends in northern peatlands (2001–2023). (a) Map of the mean decadal LAI trend, where warmer colours indicate stronger greening and cooler colours indicate browning. (b) Distribution of

https://doi.org/10.5194/egusphere-2026-109
Preprint. Discussion started: 19 February 2026

decadal trends shown as a density-scaled histogram, with bar fill indicating the dominant trend shape (linear, hat-shaped, cup-shaped). Numbers above bars are pixel counts per bin; the grey curve is the kernel density estimate, and the dashed vertical line marks zero trend.

Despite a high proportion of greening trends, we did not find a significant overall increase in LAI at the map scale between 2001 and 2023 (Table A2). Additionally, the partitioned spatial GLS indicated that greater tree cover was associated with less greening (i.e., less positive or more negative) LAI trend, conditional on continent, mapped tree canopy context, and the multi-year mean annual precipitation estimated for 2001–2023. In Asian peatlands where the nearest surrounding trees in 2001 were mapped as evergreen needleleaf, each additional +1% tree cover was associated with a mean decline of 1.06×10^{-4} $m^2m^{-2}decade^{-1}$ (Table A1). Relative to Asia, the slope was markedly steeper in North America and marginally weaker in Europe. Compared with the evergreen needleleaf tree cover, the deciduous needleleaf context mitigated this negative tree-cover effect, whereas broadleaf and mixed forests tended toward more negative slopes. Higher multi-year mean annual precipitation was associated with a less negative tree-cover slope.

After accounting for the continent, the mapped tree canopy type and cover, and precipitation in GLS, the remaining factors, such as protection status type, climate zones, and geographical coordinates, were found to be insignificant. We did not include Arctic lake drainage in the GLS model because it was present in only 2328 pixels (0.187% of the dataset). Nevertheless, pixels overlapping the drained lakes showed a higher proportion of increasing and cup-shaped LAI trends (Fig. 5). Given the limited and clustered sample, this pattern should be interpreted as exploratory and not generalised.

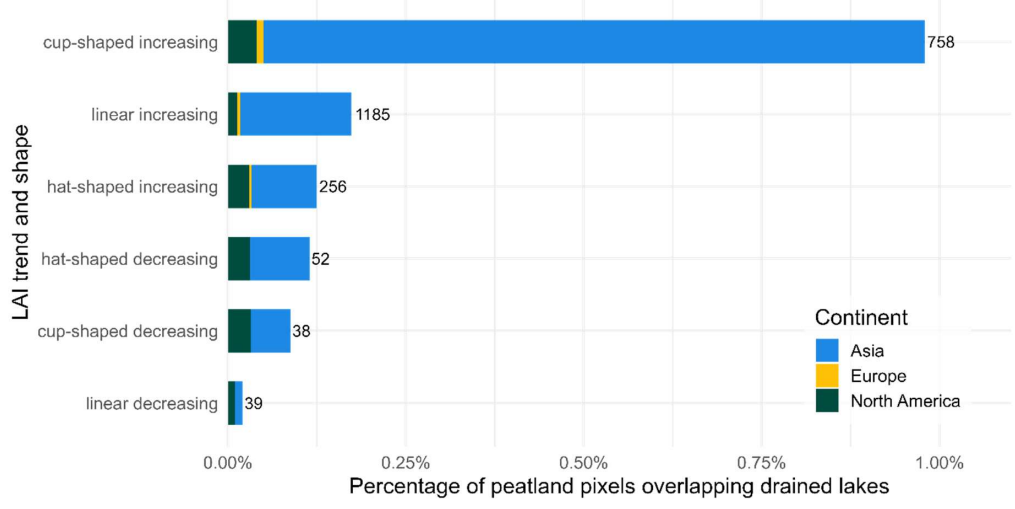

Figure 5: Proportion of peatland pixels that overlap drained-lake polygons by long-term LAI trend (increasing and decreasing) and trend-shape class. Horizontal bars indicate the share of pixels with a drained lake overlap greater than 0%; coloured segments

https://doi.org/10.5194/egusphere-2026-109
Preprint. Discussion started: 19 February 2026

denote the continental composition (Asia, Europe, North America) of the overlapping pixels. Numbers at bar ends give the count of overlapping pixels. Classes are ordered by decreasing prevalence.

5 Discussion

5.1 Long-term trends in LAI

We found that vegetation greening was observed across 77% of the studied peatlands for 2001–2023, with a greening-to-browning ratio of 3.5:1. This is broadly consistent with multi-decadal satellite records that reported widespread greening since at least the 1980s across different regions (Myneni et al., 1997; Piao et al., 2019), although the extent of greening varied with study scale and timeframe. At the global scale, greening was estimated at 27% for 2000–2017 using MODIS annual maximum FPAR (Cai et al., 2025), 40% for 1981–2017 with GIMMS and MODIS LAI (Winkler et al., 2021), 46% for 1985–2011 using GIMMS3g LAI (Forzieri et al., 2017), and up to 50% for 1982–2014 with GIMMS LAI3g, GLOBMAP LAI, and GLASS LAI (Zhu et al., 2016). Regional studies reported comparable areas of greening, including 39% in the Arctic and 41% in the boreal vegetation for 1981–2011 with GIMMS NDVI3g (Xu et al., 2013), 24% in an undisturbed Canadian forest for 1981–2011 with Landsat NDVI (Sulla-Menashe et al., 2018), and only 8.4% in West Siberia for 2000–2014 using MODIS NDVI data (Armstrong et al., 2016).

Our higher greening percentage most likely reflects methodological differences. We used the PARTS approach and, unlike many previous studies, did not threshold trends by per-pixel p-values; requiring per-pixel significance typically reduces the mapped extent of greening. Differences in data products, study periods, and data quality (Pu et al., 2024) may further explain differences between our results and other studies, yet our greening-to-browning ratio is consistent with a 3.6:1 greening-to-browning ratio in the Low Arctic observed before (Berner et al., 2020).

5.2 Influence of precipitation and air temperature on LAI

At broader scales and across many ecosystems, greening was often associated with higher precipitation (Cai et al., 2025; Forzieri et al., 2017; Piao et al., 2019). In contrast, we found a predominantly negative association between LAI and precipitation in northern peatlands (Fig. 2b). This pattern is consistent with Yuan et al. (2019), who reported a positive relationship between LAI and vapour pressure deficit over peatland-dominated areas of West Siberia and the Hudson Bay Lowlands, whereas greenness generally decreased with rising vapour pressure deficit across much of the globe (Yuan et al., 2019). Multiple mechanisms can mediate LAI-precipitation relationships at high latitudes; for example, browning in parts of the Arctic was linked to increased cloud cover (Lara et al., 2018), whereas greening arose from graminoid and shrub expansion (Berner et al., 2020; Kettridge et al., 2015; Myers-Smith et al., 2011).

In northern peatlands, this negative LAI-precipitation association aligns with hydrological controls: reduced precipitation lowers the water table, leading to peatlands drying under a warmer climate (Swindles et al., 2019). Such hydrological shifts favour the expansion of dry-habitat species (Gałka et al., 2023), for example, vascular plant expansion at the expense of

https://doi.org/10.5194/egusphere-2026-109
Preprint. Discussion started: 19 February 2026

Sphagnum where the water table falls below ~20 cm under persistently warm conditions (Keane et al., 2025). This vegetation change increases vascular leaf area and, consequently, the overall LAI of peatlands. Thus, greening in northern peatlands may reflect the expansion of vascular plants rather than enhanced *Sphagnum* growth.

It is noteworthy that multi-year mean annual precipitation, rather than air temperature, was retained in the best-fitting model. This aligns with the evidence that multi-decadal greening in high latitudes was primarily associated with rising air temperatures, resulting in growing-season lengthening and the relaxation of cold constraints (Park et al., 2020; Piao et al., 2019). However, over the past two decades, vegetation responses have been governed increasingly by moisture balance, making water availability the proximate control on canopy dynamics (Chen et al., 2025), and having facilitated the expansion of vascular plants in peatlands (Bu et al., 2011). Probably due to these moisture-driven conditions in our study region, a higher multi-year mean annual precipitation moderated the negative tree-cover slope, making it less negative (and, in sufficiently wet sites, even positive).

Given the centrality of moisture in northern peatlands, interpreting LAI dynamics requires tracking moisture conditions alongside temperature. Recent analyses indicated increased aridity across northern Eurasia (Sardans et al., 2024) and expanding heatwave coverage in the Arctic (Rantanen et al., 2024), both of which could intensify evaporative loss and further increase the expansion of vascular plants. Therefore, future work could link observed LAI trends with modelled peatland moisture, for example, using peatland-specific land-surface models (Bechtold et al., 2019), to improve detection of recent moisture-driven regime shifts in northern peatlands at the circumpolar scale.

5.3 Influence of PDO and non-linearity in LAI trends

For the first time, to our knowledge, we observed that a shift in the PDO phase might contribute to changes in vegetation trends in peatland vegetation (Fig. 3b), where a high number of breakpoints in the LAI trend occurred soon after a phase change in the PDO. This aligns with prior works showing that PDO modulates vegetation in other regions via meteorological anomalies (Guo et al., 2023; Pan et al., 2018): growing-season greenness tends to be higher during negative than positive PDO phases (Gonsamo et al., 2016). Moreover, the extremely positive PDO in 2015 resulted in higher greening, where it brought cooler, wetter conditions (central Eurasia) and browning, where it brought warmer, drier conditions (central Europe and western North America) (Bastos et al., 2017).

Regionally, the PDO-LAI relationships showed clear, region-specific signs (Fig. 3c). Under the negative PDO phase, local meteorological conditions differ by region: it is warmer and wetter in West Siberia but cooler and drier in the Baltic region and along the North American Pacific coast (Guo et al., 2023). Accordingly, in West Siberia, we observed predominantly negative LAI anomalies during the negative PDO phase (2005-2012; Fig. 3a) and a positive correlation between PDO and LAI (higher LAI in positive PDO, lower in negative PDO). In the Baltic region, we observed mostly positive LAI anomalies during negative phases of the PDO, accompanied by a negative correlation between PDO and LAI (higher LAI during negative PDO phases and lower during positive PDO phases). Along the North American Pacific coast, the cooler, drier negative phase likewise coincided with positive LAI anomalies. Taken together, these spatial patterns likely reflect a PDO-associated moisture

https://doi.org/10.5194/egusphere-2026-109
Preprint. Discussion started: 19 February 2026

anomaly, with regional modulation by other large-scale atmospheric circulation (MacIas-Fauria et al., 2012; Scholten et al., 2022). In this way, precipitation anomalies through their effect on the water table in peatlands may determine the favourable conditions for expansion and growth of vascular plants: wetter phases tend to suppress vascular canopy development, whereas drier phases favour vascular growth (Keane et al., 2025; Kettridge et al., 2015).

Beyond large-scale atmospheric circulation, permafrost thaw can also introduce decadal non-linearity in LAI trends. Frozen ground acts as a hydrological dam; thawing and thermokarst-lake drainage breaches this dam, reconfiguring drainage pathways and partially draining areas, which leads to land cover transition (Carpino et al., 2021). Consistent with this pathway, pixels overlapping mapped drained lakes showed a higher prevalence of increasing and cup-shaped LAI trajectories (Fig. 5), compatible with a vegetation shift in which initial permafrost disturbance is followed by graminoid and shrub colonisation and, locally, tree establishment after ~2–3 decades (Carpino et al., 2021). Because moderate-resolution LAI data integrates heterogeneous peatland–lake mosaics, part of the apparent LAI increase may reflect a decline in the open-water fraction rather than canopy change alone. Nevertheless, the vegetation shift associated with permafrost thaw and thermokarst-lake drainage remains poorly quantified at circumpolar scales; future work should utilise higher-resolution greenness analyses (e.g., Landsat/Sentinel-2) to study the thaw–drain–revegetate mechanism across regions.

5.4 Tree cover and LAI trends

LAI trends became more negative with increasing tree cover across partitions; however, the effect was numerically small (-1.06×10^{-4} m^2 m^{-2} $decade^{-1}$ per 1% cover increase in the Asia evergreen baseline; Table A1). This finding is consistent with that of Winkler et al. (2021), who reported browning occurring in areas with high LAI (forests) and greening in low-LAI areas, attributing forest browning to climate-change-driven water stress and disturbances, and greening in northern low-LAI ecosystems to growing season lengthening. Because that study did not include areas with high peatland density, it is essential to note that peatlands may involve additional mechanisms. For example, the loss of evergreen needleleaf trees (black spruce) can lead to counterintuitive greening trends in peatlands through reduced shadowing and species shifts (Dearborn and Baltzer, 2021).

In our study, the tree-cover slope was significantly attenuated in deciduous needleleaf contexts. This aligns with Dearborn and Baltzer (2021), who showed that larch mitigates the negative association between tree mortality and greening, and Armstrong et al. (2016), who found that larch-dominated needle-leaf forests were greening, unlike evergreen coniferous forests and evergreen-majority mixed forests in Western Siberia. Taken together, these observations may suggest that LAI increases in peatlands located near deciduous needleleaf forest could partially reflect colonisation by adjacent deciduous conifers of drying places (Kirpotin et al., 2009) in the Western Siberia taiga, where an ongoing peatland decline is happening (Kirpotin et al., 2009).

Within our dataset, North American peatlands exhibited higher baseline tree cover than Eurasian peatlands (Fig. A1), which may partly explain the stronger estimated tree-cover penalty in North America. Relative to Asia, the tree-cover coefficient yielded a total slope of -0.161×10^{-3} m^2 m^{-2} $decade^{-1}$ per 1% cover in the North American evergreen needleleaf baseline (Table

https://doi.org/10.5194/egusphere-2026-109
Preprint. Discussion started: 19 February 2026

A1). Counterintuitively, the largest positive LAI trends in North America occurred at the high end of tree cover. This can arise when partial conifer mortality and understory release increase vascular leaf area despite high initial canopy cover, as documented in boreal peatlands (Dearborn and Baltzer, 2021). In the Hudson Plains, we observed small trends in LAI, whereas Montesano et al. (2024) reported an increase in tree cover over recent decades, suggesting broader vegetation changes in the surrounding landscape. We also found a higher proportion of browning trends in North American peatlands than in Eurasian ones, in line with earlier reports of widespread browning in North American boreal forests, likely may be influenced by drought, wildfire, and insect outbreaks (Winkler et al., 2021; Xu et al., 2013). Taken together, these patterns fit a broader picture of divergent boreal trajectories in Eurasia and North America, with continued warming in North America curbing long-term productivity gains (Muccio et al., 2025).

5.5 Protected status and LAI trends

In our analysis, ~11% of the studied pixels fell within protected areas. This accords with the global estimates, where only ~17% of peatlands are protected (11% in the boreal region), substantially less than many other ecosystems (Austin et al., 2025). The protection status of peatlands did not significantly explain LAI trends. Importantly, a null association with LAI should not be construed as evidence that protection is ineffective; benefits may occur in attributes not captured by LAI (e.g., biodiversity), or at magnitudes below detectability, given the limited protected-area coverage. Moreover, legal designation alone may not buffer LAI-related dynamics because many protected areas are small and fragmented, exposed to edge effects and biological invasions, conservation actions can be uneven or ineffective, and climate change has often been overlooked in siting and management (Gatiso et al., 2022; Li et al., 2024; Ren et al., 2021). Taken together, our results may suggest that LAI trends in peatlands were more closely associated with climate exposure than with nominal protection status, underscoring the value of climate-aware management and planning (Cimatti et al., 2025).

6 Conclusions

This study quantified pan-northern greening and browning across mapped peatlands over the past two decades and examined the potential drivers of these changes. Using a sensor-independent LAI record and a spatio-temporal modelling framework, we found that canopy change was not uniformly greening but was dominated by moisture-sensitive, composition-dependent responses that were regionally modulated by decadal climate variability. More specifically:

1) 77% of northern peatlands experience net greening, but there was no significant overall increase in LAI at the map scale between 2001 and 2023.

2) LAI anomalies correlated weakly positive with air temperature and weakly negative with precipitation, consistent with hydroclimatic control of peatland canopy dynamics.

https://doi.org/10.5194/egusphere-2026-109
Preprint. Discussion started: 19 February 2026

3) Greater tree cover was associated with more negative LAI trends (less greening), this association was strongest in North America. The penalty was attenuated in deciduous needleleaf contexts and at higher multi-year precipitation, indicating interactions between canopy composition and moisture.

4) Most studied pixels showed no breakpoints. Where breakpoints occurred, they often appeared soon after PDO phase shifts. Pattern shapes varied by region: cup-shaped trends (decline then rise) were concentrated in West Siberia, while hat-shaped trends (rise then decline) were widespread across Europe, northeastern Asia, and Canada.

5) Protection status was not a significant predictor once climate and canopy covariates were considered, suggesting that nominal designation alone does not explain recent peatland LAI trajectories at this scale.

6) Pixels overlapping drained lakes were more likely to show increasing and cup-shaped LAI trends, consistent with thaw–drain–revegetate pathways.

https://doi.org/10.5194/egusphere-2026-109
Preprint. Discussion started: 19 February 2026

7 Appendices

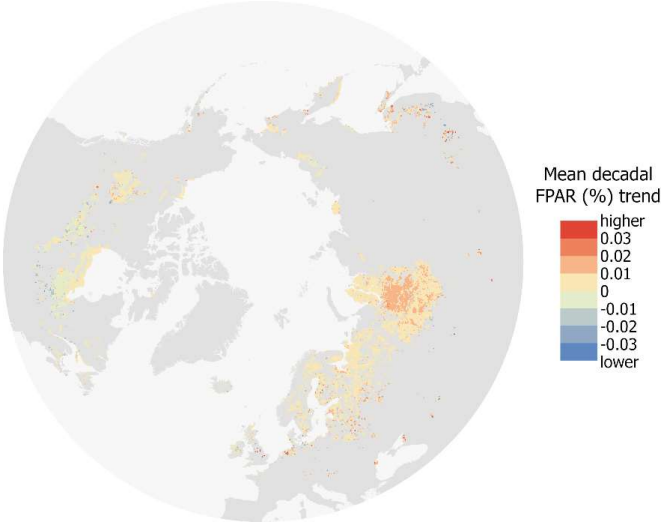

Figure A1: Spatial patterns of the mean decadal FPAR trend, where warmer colours indicate stronger greening and cooler colours indicate browning.

https://doi.org/10.5194/egusphere-2026-109
Preprint. Discussion started: 19 February 2026

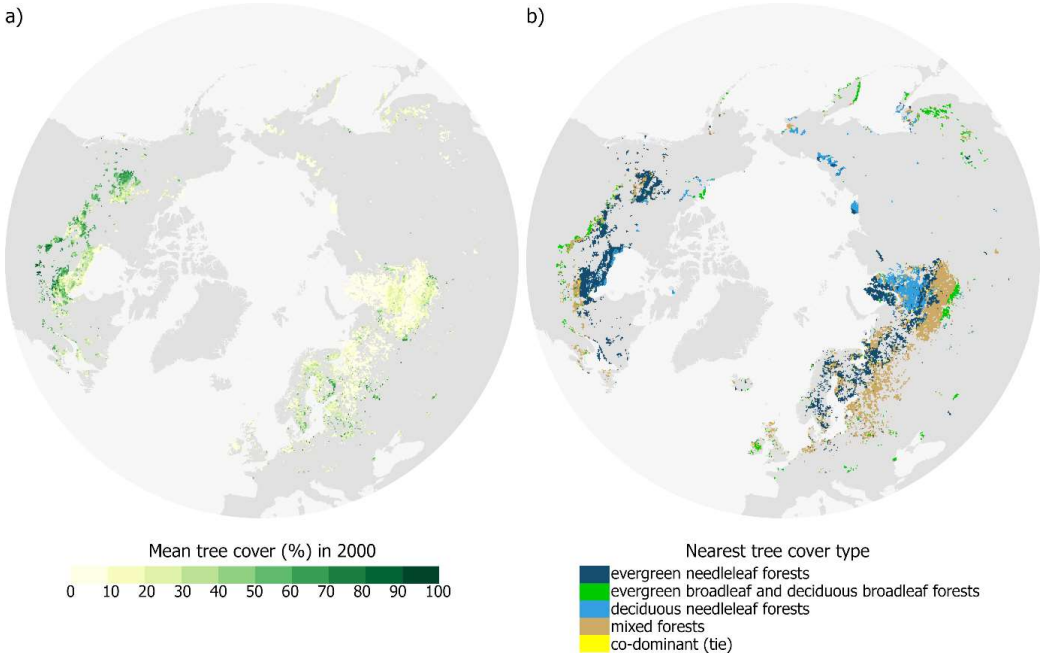

435 **Figure A2: Mean tree cover in 2000 (panel a) and the nearest type of tree cover (panel b) in the studied northern peatlands.**

https://doi.org/10.5194/egusphere-2026-109
Preprint. Discussion started: 19 February 2026

Table A1: Summary of the pooled cross-partition GLS coefficients for the best-fitted model.

$LAItrend_{8d} \sim Tree\ cover\ \times (Tree\ type + Continent + Mean\ yearly\ precipitation)$ reported on original MODIS 8-day units (m^2m^{-2} per 8-day composite). Model fit pooled over 829 disjoint 1,500-pixel partitions (exponential covariance; pooled nugget) was F(6, 1487) = 2.5813, pooled χ^2 p ≈ 1×10^{-6}, rSSE = 0.0198516, rSSR = 0.00338185. Baselines were evergreen needleleaf (Tree type) and Asia (Continent). The primary slope with respect to tree cover (per +1% cover) was negative (-2.322×10^{-7}; SE 4.231×10^{-8}; p = 4.06×10^{-8}). Two interactions dominated modulation of this slope: (i) North America × Tree cover was strongly negative (-1.208×10^{-7}; SE 1.715×10^{-8}; p = 1.88×10^{-12}), indicating steeper declines than in Asia; (ii) Tree cover × Multi-year mean annual precipitation was positive ($+8.100 \times 10^{-9}$ per mm yr^{-1}; SE 1.676×10^{-9}; p = 1.34×10^{-6}), meaning wetter conditions mitigate the negative tree-cover effect (≈ $+8.10 \times 10^{-7}$ per +100 mm yr^{-1}). Canopy composition also matters: Tree cover × Tree type 3 (deciduous needleleaf forests) attenuated the decline ($+9.044 \times 10^{-8}$; SE 2.010×10^{-8}; p = 6.80×10^{-6}), while Tree cover × Tree type classes 2 and 4 (evergreen broadleaf and deciduous broadleaf forests) and Tree cover × Tree type 5 (mixed forests) were modest and borderline (-3.875×10^{-8}, p = 0.0526; -2.121×10^{-8}, p = 0.0499).

Term	Est	SE	t.stat	p-value
(Intercept)	6.323157e-06	6.392923e-05	0.09890871	9.212108e-01
Tree cover	**−2.322120e-07**	4.231139e-08	−5.48812539	4.063013e-08
Tree type classes 2 and 4	−1.893741e-06	9.010311e-07	−2.10174818	3.557554e-02
Tree type class 3	5.582051e-07	6.437125e-07	0.86716524	3.585516e-01
Tree type class 5	9.333350e-07	4.427953e-07	2.10783419	3.504554e-02
Continent Europe	2.569953e-06	5.558160e-06	0.46231002	6.438591e-01
Continent North America	9.486842e-07	1.450199e-05	0.06541753	9.478416e-01
Multi-year mean annual precipitation for 2001-2023	−6.757034e-08	1.444677e-07	−0.46771926	6.399854e-01
Tree cover:Tree type classes 2 and 4	−3.874632e-08	1.999348e-08	−1.93794780	5.262982e-02
Tree cover:Tree type class 3	**9.043552e-08**	2.009727e-08	4.49890869	6.799462e-06
Tree cover:Tree type class 5	−2.121349e-08	1.081900e-08	−1.96070495	4.990848e-02
Tree cover:continent Europe	3.839998e-08	1.976543e-08	1.94278145	5.204280e-02
Tree cover:continent North America	**−1.208083e-07**	1.715150e-08	−7.04342533	1.876763e-12
Tree cover: Multi-year mean annual precipitation for 2001-2023	**8.099960e-09**	1.675601e-09	4.83406365	1.337898e-06

https://doi.org/10.5194/egusphere-2026-109
Preprint. Discussion started: 19 February 2026

Table A2: Summary of the pooled cross-partition GLS coefficients for the intercept-only map-level trend model.

$LAItrend_{8d} \sim 1$ reported on original MODIS 8-day units (m^2m^{-2} per 8-day composite). The pooled intercept represents the grand mean trend across all pixels. The estimate is indistinguishable from zero, indicating no detectable map-level LAI trend once spatial autocorrelation is accounted for.

Term	Est	SE	t_stat	p-value
(Intercept)	-5.050541×10^{-7}	6.962596×10^{-5}	−0.0072538	0.9942123

https://doi.org/10.5194/egusphere-2026-109
Preprint. Discussion started: 19 February 2026

Code, data, or code and data availability

The LAI/FPAR CDR is openly available at https://doi.org/10.5281/zenodo.8076540.

Competing interests

The authors declare no conflicts of interest.

Author contributions

Iuliia Burdun: Conceptualization, Methodology, Software, Validation, Formal analysis, Data curation, Writing – original draft, Visualization.
Jiabin Pu: Writing – review & editing, Data curation.
Ranga B. Myneni: Writing – review & editing, Data curation.
Miina Rautiainen: Conceptualization, Methodology, Resources, Data curation, Writing – review & editing, Supervision, Project administration, Funding acquisition.

Disclaimer

Copernicus Publications remains neutral with regard to jurisdictional claims made in the text, published maps, institutional affiliations, or any other geographical representation in this paper. While Copernicus Publications makes every effort to include appropriate place names, the final responsibility lies with the authors. Views expressed in the text are those of the authors and do not necessarily reflect the views of the publisher.

Acknowledgements

We gratefully acknowledge the CSC—IT Center for Science, Finland, for providing computational resources through the Puhti supercomputer. Iuliia Burdun acknowledged the use of ChatGPT (OpenAI) for improving the flow of the manuscript text.

Financial support

The study was mainly funded by the Research Council of Finland (Grant: PEATSPEC 3341963/ Miina Rautiainen and Iuliia Burdun). Iuliia Burdun acknowledge FWO, which has co-financed the underlying research, Junior Postdoctoral Fellowship 12A5O24N.

https://doi.org/10.5194/egusphere-2026-109
Preprint. Discussion started: 19 February 2026

References

Anon: Global Peatland Database - Greifswald Mire Centre, https://greifswaldmoor.de/global-peatland-database-en.html, 2024.

Pacific Decadal Oscillation (PDO) | National Centers for Environmental Information (NCEI): https://www.ncei.noaa.gov/access/monitoring/pdo/, last access: 11 August 2025.

Armstrong, A., Alcaraz-Segura, D., Raynolds, M., -, al, Phillips, T. J., W Bonfils -, C. J., Miles, V. V, and Esau, I.: Spatial heterogeneity of greening and browning between and within bioclimatic zones in northern West Siberia, Environmental Research Letters, 11, 115002, https://doi.org/10.1088/1748-9326/11/11/115002, 2016.

Austin, K. G., Elsen, P. R., Coronado, E. N. H., DeGemmis, A., Gallego-Sala, A. V., Harris, L., Kretser, H. E., Melton, J. R., Murdiyarso, D., Sasmito, S. D., Swails, E., Wijaya, A., Winton, R. S., and Zarin, D.: Mismatch Between Global Importance of Peatlands and the Extent of Their Protection, Conserv Lett, 18, e13080, https://doi.org/10.1111/CONL.13080, 2025.

Backéus, I., Gunnarsson, U., and Strömquist, L.: Bog vegetation re-mapped after 63 and 103 years:expansion of Rhynchospora alba (Studies on Skagershultsmossen 2), Mires and Peat, 29, 16, 2023.

Bansal, S., der Burg, M. P. van, Fern, R. R., Jones, J. W., Lo, R., McKenna, O. P., Tangen, B. A., Zhang, Z., and Gleason, R. A.: Large increases in methane emissions expected from North America's largest wetland complex, Sci Adv, 9, https://doi.org/https://doi.org/10.1126/sciadv.ade1112, 2023.

Barichivich, J., Briffa, K. R., Myneni, R. B., Osborn, T. J., Melvin, T. M., Ciais, P., Piao, S., and Tucker, C.: Large-scale variations in the vegetation growing season and annual cycle of atmospheric CO2 at high northern latitudes from 1950 to 2011, Glob Chang Biol, 19, 3167–3183, https://doi.org/10.1111/GCB.12283, 2013.

Bastos, A., Ciais, P., Park, T., Zscheischler, J., Yue, C., Barichivich, J., Myneni, R. B., Peng, S., Piao, S., and Zhu, Z.: Was the extreme Northern Hemisphere greening in 2015 predictable?, Environmental Research Letters, 12, 044016, https://doi.org/10.1088/1748-9326/AA67B5, 2017.

Bechtold, M., De Lannoy, G., Koster, R. D., Reichle, R. H., Mahanama, S., Bleuten, W., Bourgault, M. A., Brümmer, C., Burdun, I., Desai, A. R., Devito, K., Grünwald, T., Grygoruk, M., Humphreys, E. R., Klatt, J., Kurbatova, J., Lohila, A., Munir, T. M., Nilsson, M. B., Price, J. S., Röhl, M., Schneider, A., and Tiemeyer, B.: PEAT-CLSM: A Specific Treatment of Peatland Hydrology in the NASA Catchment Land Surface Model, J Adv Model Earth Syst, 11, 1–33, https://doi.org/10.1029/2018MS001574, 2019.

Beck, H. E., Zimmermann, N. E., McVicar, T. R., Vergopolan, N., Berg, A., and Wood, E. F.: Present and future Köppen-Geiger climate classification maps at 1-km resolution, Scientific Data 2018 5:1, 5, 1–12, https://doi.org/10.1038/sdata.2018.214, 2018.

Berner, L. T., Massey, R., Jantz, P., Forbes, B. C., Macias-Fauria, M., Myers-Smith, I., Kumpula, T., Gauthier, G., Andreu-Hayles, L., Gaglioti, B. V., Burns, P., Zetterberg, P., D'Arrigo, R., and Goetz, S. J.: Summer warming explains widespread but not uniform greening in the Arctic tundra biome, Nature Communications 2020 11:1, 11, 1–12, https://doi.org/10.1038/s41467-020-18479-5, 2020.

https://doi.org/10.5194/egusphere-2026-109
Preprint. Discussion started: 19 February 2026

Bragazza, L., Parisod, J., Buttler, A., and Bardgett, R. D.: Biogeochemical plant–soil microbe feedback in response to climate warming in peatlands, Nature Climate Change 2013 3:3, 3, 273–277, https://doi.org/10.1038/nclimate1781, 2012.

Bu, Z., Hans, J., Li, H., Zhao, G., Zheng, X., Ma, J., and Zeng, J.: The response of peatlands to climate warming: A review, Acta Ecologica Sinica, 31, 157–162, https://doi.org/10.1016/J.CHNAES.2011.03.006, 2011.

Cai, W., Zhu, Z., Harrison, S. P., Ryu, Y., Wang, H., Zhou, B., and Prentice, I. C.: A unifying principle for global greenness patterns and trends, Communications Earth & Environment 2025 6:1, 6, 1–11, https://doi.org/10.1038/s43247-025-01992-0, 2025.

Campbell, C., Granath, G., and Rydin, H.: Climatic drivers of Sphagnum species distributions, Front Biogeogr, 13, https://doi.org/10.21425/F5FBG51146, 2021.

Carpino, O., Haynes, K., Connon, R., Craig, J., Devoie, É., and Quinton, W.: Long-term climate-influenced land cover change in discontinuous permafrost peatland complexes, Hydrol Earth Syst Sci, 25, 3301–3317, https://doi.org/10.5194/HESS-25-3301-2021, 2021.

Chen, L., Brun, P., Buri, P., Fatichi, S., Gessler, A., McCarthy, M. J., Pellicciotti, F., Stocker, B., and Karger, D. N.: Global increase in the occurrence and impact of multiyear droughts, Science (1979), 387, 278–284, https://doi.org/https://doi.org/10.1126/science.ado4245, 2025.

Chen, Y., Cheng, X., Liu, A., Chen, Q., and Wang, C.: Tracking lake drainage events and drained lake basin vegetation dynamics across the Arctic, Nature Communications 2023 14:1, 14, 1–18, https://doi.org/10.1038/s41467-023-43207-0, 2023.

Cimatti, M., Mezzanotte, V., Heikkinen, R. K., Hällfors, M. H., Karger, D. N., and Di Marco, M.: The Accelerating Exposure of European Protected Areas to Climate Change, Glob Chang Biol, 31, e70261, https://doi.org/10.1111/GCB.70261, 2025.

Dearborn, K. D. and Baltzer, J. L.: Unexpected greening in a boreal permafrost peatland undergoing forest loss is partially attributable to tree species turnover, Glob Chang Biol, 27, 2867–2882, https://doi.org/10.1111/GCB.15608, 2021.

Elmendorf, S. C., Henry, G. H. R., Hollister, R. D., Björk, R. G., Boulanger-Lapointe, N., Cooper, E. J., Cornelissen, J. H. C., Day, T. A., Dorrepaal, E., Elumeeva, T. G., Gill, M., Gould, W. A., Harte, J., Hik, D. S., Hofgaard, A., Johnson, D. R., Johnstone, J. F., Jónsdóttir, I. S., Jorgenson, J. C., Klanderud, K., Klein, J. A., Koh, S., Kudo, G., Lara, M., Lévesque, E., Magnússon, B., May, J. L., Mercado-Díaz, J. A., Michelsen, A., Molau, U., Myers-Smith, I. H., Oberbauer, S. F., Onipchenko, V. G., Rixen, C., Martin Schmidt, N., Shaver, G. R., Spasojevic, M. J., Pórhallsdóttir, P. E., Tolvanen, A., Troxler, T., Tweedie, C. E., Villareal, S., Wahren, C. H., Walker, X., Webber, P. J., Welker, J. M., and Wipf, S.: Plot-scale evidence of tundra vegetation change and links to recent summer warming, Nature Climate Change 2012 2:6, 2, 453–457, https://doi.org/10.1038/nclimate1465, 2012.

Fick, S. E. and Hijmans, R. J.: WorldClim 2: new 1-km spatial resolution climate surfaces for global land areas, International Journal of Climatology, 37, 4302–4315, https://doi.org/10.1002/JOC.5086, 2017.

Fluet-Chouinard, E., Stocker, B. D., Zhang, Z., Malhotra, A., Melton, J. R., Poulter, B., Kaplan, J. O., Goldewijk, K. K., Siebert, S., Minayeva, T., Hugelius, G., Joosten, H., Barthelmes, A., Prigent, C., Aires, F., Hoyt, A. M., Davidson, N.,

https://doi.org/10.5194/egusphere-2026-109
Preprint. Discussion started: 19 February 2026

Finlayson, C. M., Lehner, B., Jackson, R. B., and McIntyre, P. B.: Extensive global wetland loss over the past three centuries, Nature 2023 614:7947, 614, 281–286, https://doi.org/10.1038/s41586-022-05572-6, 2023.

Forzieri, G., Alkama, R., Miralles, D. G., and Cescatti, A.: Satellites reveal contrasting responses of regional climate to the widespread greening of Earth, Science (1979), 356, 1180–1184, https://doi.org/https://doi.org/10.1126/science.aal1727, 2017.

Gałka, M., Diaconu, A. C., Cwanek, A., Hedenäs, L., Knorr, K. H., Kołaczek, P., Łokas, E., Obremska, M., Swindles, G. T., and Feurdean, A.: Climate-induced hydrological fluctuations shape Arctic Alaskan peatland plant communities, Science of The Total Environment, 905, 167381, https://doi.org/10.1016/J.SCITOTENV.2023.167381, 2023.

Gatiso, T. T., Kulik, L., Bachmann, M., Bonn, A., Bösch, L., Eirdosh, D., Freytag, A., Hanisch, S., Heurich, M., Sop, T., Wesche, K., Winter, M., and Kühl, H. S.: Effectiveness of protected areas influenced by socio-economic context, Nat Sustain, 5, 861–868, https://doi.org/https://doi.org/10.1038/s41893-022-00932-6, 2022.

Gonsamo, A., Chen, J. M., and Lombardozzi, D.: Global vegetation productivity response to climatic oscillations during the satellite era, Glob Chang Biol, 22, 3414–3426, https://doi.org/10.1111/GCB.13258, 2016.

Guo, Z., Sun, C., Fu, Y., Liu, Y., Wei, T., and Lou, W.: Different trends of vegetation activity over northern extratropics during two multidecadal warming periods in the 20th century, Glob Planet Change, 227, 104181, https://doi.org/10.1016/J.GLOPLACHA.2023.104181, 2023.

Hansen, M. C., Potapov, P. V., Moore, R., Hancher, M., Turubanova, S. A., Tyukavina, A., Thau, D., Stehman, S. V., Goetz, S. J., Loveland, T. R., Kommareddy, A., Egorov, A., Chini, L., Justice, C. O., and Townshend, J. R. G.: High-resolution global maps of 21st-century forest cover change, Science (1979), 342, 850–853, https://doi.org/https://doi.org/10.1126/science.1244693, 2013.

Hersbach, H., Bell, B., Berrisford, P., Hirahara, S., Horányi, A., Muñoz-Sabater, J., Nicolas, J., Peubey, C., Radu, R., Schepers, D., Simmons, A., Soci, C., Abdalla, S., Abellan, X., Balsamo, G., Bechtold, P., Biavati, G., Bidlot, J., Bonavita, M., Chiara, G., Dahlgren, P., Dee, D., Diamantakis, M., Dragani, R., Flemming, J., Forbes, R., Fuentes, M., Geer, A., Haimberger, L., Healy, S., Hogan, R. J., Hólm, E., Janisková, M., Keeley, S., Laloyaux, P., Lopez, P., Lupu, C., Radnoti, G., Rosnay, P., Rozum, I., Vamborg, F., Villaume, S., and Thépaut, J.: The ERA5 Global Reanalysis, Quarterly Journal of the Royal Meteorological Society, 1–51, https://doi.org/10.1002/qj.3803, 2020.

Higgins, S. I., Conradi, T., and Muhoko, E.: Shifts in vegetation activity of terrestrial ecosystems attributable to climate trends, Nature Geoscience 2023 16:2, 16, 147–153, https://doi.org/10.1038/s41561-022-01114-x, 2023.

Hu, S., Niu, Z., Chen, Y., Li, L., and Zhang, H.: Global wetlands: Potential distribution, wetland loss, and status, Science of The Total Environment, 586, 319–327, https://doi.org/10.1016/J.SCITOTENV.2017.02.001, 2017.

Hugelius, G., Loisel, J., Chadburn, S., Jackson, R. B., Jones, M., MacDonald, G., Marushchak, M., Olefeldt, D., Packalen, M., Siewert, M. B., Treat, C., Turetsky, M., Voigt, C., and Yu, Z.: Large stocks of peatland carbon and nitrogen are vulnerable to permafrost thaw, Proc Natl Acad Sci U S A, 117, 20438–20446, https://doi.org/https://doi.org/10.1073/pnas.1916387117, 2020.

https://doi.org/10.5194/egusphere-2026-109
Preprint. Discussion started: 19 February 2026

Ives, A. R., Zhu, L., Wang, F., Zhu, J., Morrow, C. J., and Radeloff, V. C.: Statistical inference for trends in spatiotemporal data, Remote Sens Environ, 266, 112678, https://doi.org/10.1016/J.RSE.2021.112678, 2021.

de Jong, R., Verbesselt, J., Schaepman, M. E., and de Bruin, S.: Trend changes in global greening and browning: Contribution of short-term trends to longer-term change, Glob Chang Biol, 18, 642–655, https://doi.org/10.1111/j.1365-2486.2011.02578.x, 2012.

Keane, B., Alderson, D. M., Clay, G. D., Evans, M. G., Field, C. D., Johnston, A., Limpens, J., McCarter, C. P. R., Overtoom, N., Ritson, J. P., Robroek, B. J. M., Rochefort, L., Shuttleworth, E. L., Telgenkamp, Y., Turetsky, M. R., and Waddington, J. M.: The effects of drought on Sphagnum moss species and the implications for hydrology in peatlands, New Phytologist, 247, 2003–2021, https://doi.org/10.1111/NPH.70361, 2025.

Kettridge, N., Turetsky, M. R., Sherwood, J. H., Thompson, D. K., Miller, C. A., Benscoter, B. W., Flannigan, M. D., Wotton, B. M., and Waddington, J. M.: Moderate drop in water table increases peatland vulnerability to post-fire regime shift, Sci Rep, 5, 8063, https://doi.org/10.1038/SREP08063;TECHMETA, 2015.

Kirpotin, S. N., Berezin, A., Bazanov, V., Polishchuk, Y., Vorobiov, S., Mironycheva-Tokoreva, N., Kosykh, N., Volkova, I., Dupre, B., Pokrovsky, O., Kouraev, A., Zakharova, E., Shirokova, L., Mognard, N., Biancamaria, S., Viers, J., and Kolmakova, M.: Western Siberia wetlands as indicator and regulator of climate change on the global scale, International Journal of Environmental Studies, 66, 409–421, https://doi.org/10.1080/00207230902753056, 2009.

Kolari, T. H. M., Korpelainen, P., Kumpula, T., and Tahvanainen, T.: Accelerated vegetation succession but no hydrological change in a boreal fen during 20 years of recent climate change, Ecol Evol, 11, 7602–7621, https://doi.org/10.1002/ECE3.7592, 2021.

Lara, M. J., Nitze, I., Grosse, G., Martin, P., and David McGuire, A.: Reduced arctic tundra productivity linked with landform and climate change interactions, Sci Rep, 8, 1–10, https://doi.org/10.1038/S41598-018-20692-8;TECHMETA=134,141;SUBJMETA=1144,158,2165,631,704;KWRD=CLIMATE-CHANGE+ECOLOGY,ECOLOGICAL+MODELLING, 2018.

Li, G., Fang, C., Watson, J. E. M., Sun, S., Qi, W., Wang, Z., and Liu, J.: Mixed effectiveness of global protected areas in resisting habitat loss, Nature Communications 2024 15:1, 15, 1–17, https://doi.org/10.1038/s41467-024-52693-9, 2024.

Lian, X., Piao, S., Li, L. Z. X., Li, Y., Huntingford, C., Ciais, P., Cescatti, A., Janssens, I. A., Peñuelas, J., Buermann, W., Chen, A., Li, X., Myneni, R. B., Wang, X., Wang, Y., Yang, Y., Zeng, Z., Zhang, Y., and McVicar, T. R.: Summer soil drying exacerbated by earlier spring greening of northern vegetation, Sci Adv, 6, https://doi.org/https://doi.org/10.1126/sciadv.aax0255, 2020.

Liu, X., Chen, Y., Li, Z., and Li, Y.: Greening in the middle and high latitudes in the Northern Hemisphere is determined by changes in the growth rate of natural vegetation during the growing season, Ecol Indic, 155, 111025, https://doi.org/10.1016/J.ECOLIND.2023.111025, 2023.

https://doi.org/10.5194/egusphere-2026-109
Preprint. Discussion started: 19 February 2026

Ma, X. Y., Xu, H., Cao, Z. Y., Shu, L., and Zhu, R. L.: Will climate change cause the global peatland to expand or contract? Evidence from the habitat shift pattern of Sphagnum mosses, Glob Chang Biol, 28, 6419–6432, https://doi.org/10.1111/GCB.16354, 2022.

MacIas-Fauria, M., Forbes, B. C., Zetterberg, P., and Kumpula, T.: Eurasian Arctic greening reveals teleconnections and the potential for structurally novel ecosystems, Nat Clim Chang, 2, 613–618, https://doi.org/10.1038/NCLIMATE1558;SUBJMETA, 2012.

Montesano, P. M., Frost, M., Li, J., Carroll, M., Neigh, C. S. R., Macander, M. J., Sexton, J. O., and Frost, G. V.: A shift in transitional forests of the North American boreal will persist through 2100, Commun Earth Environ, 5, 1–10, https://doi.org/10.1038/S43247-024-01454-Z;SUBJMETA, 2024.

Muccio, D., Keppel-Aleks, G., and Parazoo, N.: Contrasting Temperature Sensitivity of Boreal Forest Productivity in North America and Eurasia, J Geophys Res Biogeosci, 130, e2024JG008634, https://doi.org/10.1029/2024JG008634, 2025.

Myers-Smith, I. H., Forbes, B. C., Wilmking, M., Hallinger, M., Lantz, T., Blok, D., Tape, K. D., MacIas-Fauria, M., Sass-Klaassen, U., Lévesque, E., Boudreau, S., Ropars, P., Hermanutz, L., Trant, A., Collier, L. S., Weijers, S., Rozema, J., Rayback, S. A., Schmidt, N. M., Schaepman-Strub, G., Wipf, S., Rixen, C., Ménard, C. B., Venn, S., Goetz, S., Andreu-Hayles, L., Elmendorf, S., Ravolainen, V., Welker, J., Grogan, P., Epstein, H. E., and Hik, D. S.: Shrub expansion in tundra ecosystems: dynamics, impacts and research priorities, Environmental Research Letters, 6, 045509, https://doi.org/10.1088/1748-9326/6/4/045509, 2011.

Myers-Smith, I. H., Kerby, J. T., Phoenix, G. K., Bjerke, J. W., Epstein, H. E., Assmann, J. J., John, C., Andreu-Hayles, L., Angers-Blondin, S., Beck, P. S. A., Berner, L. T., Bhatt, U. S., Bjorkman, A. D., Blok, D., Bryn, A., Christiansen, C. T., Cornelissen, J. H. C., Cunliffe, A. M., Elmendorf, S. C., Forbes, B. C., Goetz, S. J., Hollister, R. D., de Jong, R., Loranty, M. M., Macias-Fauria, M., Maseyk, K., Normand, S., Olofsson, J., Parker, T. C., Parmentier, F. J. W., Post, E., Schaepman-Strub, G., Stordal, F., Sullivan, P. F., Thomas, H. J. D., Tømmervik, H., Treharne, R., Tweedie, C. E., Walker, D. A., Wilmking, M., and Wipf, S.: Complexity revealed in the greening of the Arctic, Nature Climate Change 2020 10:2, 10, 106–117, https://doi.org/10.1038/s41558-019-0688-1, 2020.

Myneni, R. B., Keeling, C. D., Tucker, C. J., Asrar, G., and Nemani, R. R.: Increased plant growth in the northern high latitudes from 1981 to 1991, Nature, 386, 698–702, https://doi.org/10.1038/386698A0;KWRD, 1997.

Natural Earth vector and raster map data: https://www.naturalearthdata.com/, last access: 11 August 2025.

Oke, T. A. and Hager, H. A.: Assessing environmental attributes and effects of climate change on Sphagnum peatland distributions in North America using single- and multi-species models, PLoS One, 12, e0175978, https://doi.org/10.1371/JOURNAL.PONE.0175978, 2017.

Oke, T. A., Hager, H. A., Tobi Oke, C. A., and Jordan, G.: Plant community dynamics and carbon sequestration in Sphagnum-dominated peatlands in the era of global change, Global Ecology and Biogeography, 29, 1610–1620, https://doi.org/10.1111/GEB.13152, 2020.

OpenStreetMap: https://www.openstreetmap.org/copyright, last access: 11 August 2025.

https://doi.org/10.5194/egusphere-2026-109
Preprint. Discussion started: 19 February 2026

Pan, N., Feng, X., Fu, B., Wang, S., Ji, F., and Pan, S.: Increasing global vegetation browning hidden in overall vegetation greening: Insights from time-varying trends, Remote Sens Environ, 214, 59–72, https://doi.org/10.1016/J.RSE.2018.05.018, 2018.

Park, H., Jeong, S., and Peñuelas, J.: Accelerated rate of vegetation green-up related to warming at northern high latitudes, Glob Chang Biol, 26, 6190–6202, https://doi.org/10.1111/GCB.15322, 2020.

Piao, S., Wang, X., Park, T., Chen, C., Lian, X., He, Y., Bjerke, J. W., Chen, A., Ciais, P., Tømmervik, H., Nemani, R. R., and Myneni, R. B.: Characteristics, drivers and feedbacks of global greening, Nature Reviews Earth & Environment 2019 1:1, 1, 14–27, https://doi.org/10.1038/s43017-019-0001-x, 2019.

Ploton, P., Mortier, F., Réjou-Méchain, M., Barbier, N., Picard, N., Rossi, V., Dormann, C., Cornu, G., Viennois, G., Bayol, N., Lyapustin, A., Gourlet-Fleury, S., and Pélissier, R.: Spatial validation reveals poor predictive performance of large-scale ecological mapping models, Nat Commun, 11, 1–11, https://doi.org/10.1038/s41467-020-18321-y, 2020.

Pu, J., Yan, K., Roy, S., Zhu, Z., Rautiainen, M., Knyazikhin, Y., and Myneni, R. B.: Sensor-independent LAI/FPAR CDR: Reconstructing a global sensor-independent climate data record of MODIS and VIIRS LAI/FPAR from 2000 to 2022, Earth Syst Sci Data, 16, 15–34, https://doi.org/10.5194/ESSD-16-15-2024, 2024.

Qiu, C., Ciais, P., Zhu, D., Guenet, B., Chang, J., Chaudhary, N., Kleinen, T., Li, X. Y., Müller, J., Xi, Y., Zhang, W., Ballantyne, A., Brewer, S. C., Brovkin, V., Charman, D. J., Gustafson, A., Gallego-Sala, A. V., Gasser, T., Holden, J., Joos, F., Kwon, M. J., Lauerwald, R., Miller, P. A., Peng, S., Page, S., Smith, B., Stocker, B. D., Sannel, A. B. K., Salmon, E., Schurgers, G., Shurpali, N. J., Wårlind, D., and Westermann, S.: A strong mitigation scenario maintains climate neutrality of northern peatlands, One Earth, 5, 86–97, https://doi.org/10.1016/j.oneear.2021.12.008, 2022.

Rantanen, M., Kämäräinen, M., Luoto, M., and Aalto, J.: Manifold increase in the spatial extent of heatwaves in the terrestrial Arctic, Commun Earth Environ, 5, 1–8, https://doi.org/https://doi.org/10.1038/s43247-024-01750-8, 2024.

Ren, J., Chen, J., Xu, C., van de Koppel, J., Thomsen, M. S., Qiu, S., Cheng, F., Song, W., Liu, Q. X., Xu, C., Bai, J., Zhang, Y., Cui, B., Bertness, M. D., Silliman, B. R., Li, B., and He, Q.: An invasive species erodes the performance of coastal wetland protected areas, Sci Adv, 7, 8943–8956, https://doi.org/https://doi.org/10.1126/sciadv.abi8943, 2021.

Sardans, J., Miralles, A., Tariq, A., Zeng, F., Wang, R., and Peñuelas, J.: Growing aridity poses threats to global land surface, Commun Earth Environ, 5, 1–8, https://doi.org/10.1038/S43247-024-01935-1;TECHMETA=10,9;SUBJMETA=106,158,631,704;KWRD=CLIMATE+SCIENCES,ECOLOGY, 2024.

Scholten, R. C., Coumou, D., Luo, F., and Veraverbeke, S.: Early snowmelt and polar jet dynamics co-influence recent extreme Siberian fire seasons, Science (1979), 378, 1005–1009, https://doi.org/10.1126/SCIENCE.ABN4419, 2022.

Sturm, M., Racine, C., and Tape, K.: Increasing shrub abundance in the Arctic, Nature 2001 411:6837, 411, 546–547, https://doi.org/10.1038/35079180, 2001.

Sulla-Menashe, D., Woodcock, C. E., and Friedl, M. A.: Canadian boreal forest greening and browning trends: an analysis of biogeographic patterns and the relative roles of disturbance versus climate drivers, Environmental Research Letters, 13, 014007, https://doi.org/10.1088/1748-9326/AA9B88, 2018.

https://doi.org/10.5194/egusphere-2026-109
Preprint. Discussion started: 19 February 2026

Swindles, G. T., Morris, P. J., Mullan, D. J., Payne, R. J., Roland, T. P., Amesbury, M. J., Lamentowicz, M., Turner, T. E., Gallego-Sala, A., Sim, T., Barr, I. D., Blaauw, M., Blundell, A., Chambers, F. M., Charman, D. J., Feurdean, A., Galloway, J. M., Gałka, M., Green, S. M., Kajukało, K., Karofeld, E., Korhola, A., Lamentowicz, Ł., Langdon, P., Marcisz, K., Mauquoy, D., Mazei, Y. A., McKeown, M. M., Mitchell, E. A. D., Novenko, E., Plunkett, G., Roe, H. M., Schoning, K., Sillasoo, Ü., Tsyganov, A. N., van der Linden, M., Väliranta, M., and Warner, B.: Widespread drying of European peatlands in recent centuries, Nat Geosci, 12, 922–928, https://doi.org/10.1038/s41561-019-0462-z, 2019.

Sytiuk, A., Hamard, S., Céréghino, R., Dorrepaal, E., Geissel, H., Küttim, M., Lamentowicz, M., Tuittila, E. S., and Jassey, V. E. J.: Linkages between Sphagnum metabolites and peatland CO2 uptake are sensitive to seasonality in warming trends, New Phytologist, 237, 1164–1178, https://doi.org/10.1111/NPH.18601, 2023.

United Nations Environment Programme: Global Peatlands Assessment: The State of the World's Peatlands | UNEP - UN Environment Programme, Nairobi, 2022.

Väliranta, M., Salojärvi, N., Vuorsalo, A., Juutinen, S., Korhola, A., Luoto, M., and Tuittila, E. S.: Holocene fen–bog lhttps://doi.org/https://doi.org/10.1177/0959683616670471, 2017.

Virkkala, A. M., Rogers, B. M., Watts, J. D., Arndt, K. A., Potter, S., Wargowsky, I., Schuur, E. A. G., See, C. R., Mauritz, M., Boike, J., Bret-Harte, M. S., Burke, E. J., Burrell, A., Chae, N., Chatterjee, A., Chevallier, F., Christensen, T. R., Commane, R., Dolman, H., Edgar, C. W., Elberling, B., Emmerton, C. A., Euskirchen, E. S., Feng, L., Göckede, M., Grelle, A., Helbig, M., Holl, D., Järveoja, J., Karsanaev, S. V., Kobayashi, H., Kutzbach, L., Liu, J., Luijkx, I. T., López-Blanco, E., Lunneberg, K., Mammarella, I., Marushchak, M. E., Mastepanov, M., Matsuura, Y., Maximov, T. C., Merbold, L., Meyer, G., Nilsson, M. B., Niwa, Y., Oechel, W., Palmer, P. I., Park, S. J., Parmentier, F. J. W., Peichl, M., Peters, W., Petrov, R., Quinton, W., Rödenbeck, C., Sachs, T., Schulze, C., Sonnentag, O., St. Louis, V. L., Tuittila, E. S., Ueyama, M., Varlagin, A., Zona, D., and Natali, S. M.: Wildfires offset the increasing but spatially heterogeneous Arctic–boreal CO2 uptake, Nat Clim Chang, 15, 188–195, https://doi.org/https://doi.org/10.1038/s41558-024-02234-5, 2025.

Winkler, A. J., Myneni, R. B., Alexandrov, G. A., and Brovkin, V.: Earth system models underestimate carbon fixation by plants in the high latitudes, Nature Communications 2019 10:1, 10, 1–8, https://doi.org/10.1038/s41467-019-08633-z, 2019.

Winkler, A. J., Myneni, R. B., Hannart, A., Sitch, S., Haverd, V., Lombardozzi, D., Arora, V. K., Pongratz, J., Nabel, J. E. M. leS., Goll, D. S., Kato, E., Tian, H., Arneth, A., Friedlingstein, P., Jain, A. K., Zaehle, S., and Brovkin, V.: Slowdown of the greening trend in natural vegetation with further rise in atmospheric CO2, Biogeosciences, 18, 4985–5010, https://doi.org/10.5194/BG-18-4985-2021, 2021.

Xu, J., Morris, P., Liu, J., and Holden, J.: PEATMAP: Refining estimates of global peatland distribution based on a meta-analysis, Catena (Amst), 160, 134–140, https://doi.org/10.1016/j.catena.2017.09.010, 2018.

Xu, L., Myneni, R. B., Chapin, F. S., Callaghan, T. V., Pinzon, J. E., Tucker, C. J., Zhu, Z., Bi, J., Ciais, P., Tømmervik, H., Euskirchen, E. S., Forbes, B. C., Piao, S. L., Anderson, B. T., Ganguly, S., Nemani, R. R., Goetz, S. J., Beck, P. S. A., Bunn, A. G., Cao, C., and Stroeve, J. C.: Temperature and vegetation seasonality diminishment over northern lands, Nature Climate Change 2013 3:6, 3, 581–586, https://doi.org/10.1038/nclimate1836, 2013.

https://doi.org/10.5194/egusphere-2026-109
Preprint. Discussion started: 19 February 2026

Yuan, K., Li, F., McNicol, G., Chen, M., Hoyt, A., Knox, S., Riley, W. J., Jackson, R., and Zhu, Q.: Boreal–Arctic wetland methane emissions modulated by warming and vegetation activity, Nat Clim Chang, 14, 282–288, https://doi.org/https://doi.org/10.1038/s43247-024-01935-1, 2024.

Yuan, W., Zheng, Y., Piao, S., Ciais, P., Lombardozzi, D., Wang, Y., Ryu, Y., Chen, G., Dong, W., Hu, Z., Jain, A. K., Jiang, C., Kato, E., Li, S., Lienert, S., Liu, S., Nabel, J. E. M. S., Qin, Z., Quine, T., Sitch, S., Smith, W. K., Wang, F., Wu, C., Xiao, Z., and Yang, S.: Increased atmospheric vapor pressure deficit reduces global vegetation growth, Sci Adv, 5, https://doi.org/10.1126/SCIADV.AAX1396, 2019.

Zhu, Z., Piao, S., Myneni, R. B., Huang, M., Zeng, Z., Canadell, J. G., Ciais, P., Sitch, S., Friedlingstein, P., Arneth, A., Cao, C., Cheng, L., Kato, E., Koven, C., Li, Y., Lian, X., Liu, Y., Liu, R., Mao, J., Pan, Y., Peng, S., Peuelas, J., Poulter, B., Pugh, T. A. M., Stocker, B. D., Viovy, N., Wang, X., Wang, Y., Xiao, Z., Yang, H., Zaehle, S., and Zeng, N.: Greening of the Earth and its drivers, Nature Climate Change 2016 6:8, 6, 791–795, https://doi.org/10.1038/nclimate3004, 2016.